



Mesenchymal stem-cell-derived microvesicles ameliorate MPTP-induced neurotoxicity in mice: a role of the gut–microbiota–brain axis

Yaoyu Pu¹ · QiuHong Wu¹ · Qiuping Zhang¹ · Tianwen Huang¹ · Ji Wen¹ · Long Wei² · Kenji Hashimoto³ · Yi Liu¹

Received: 16 September 2022 / Accepted: 26 February 2023 / Published online: 7 March 2023
© The Author(s), under exclusive licence to Springer-Verlag GmbH Germany, part of Springer Nature 2023

Abstract

Rationale Parkinson’s disease (PD) is a chronic and progressive neurodegenerative disorder. Increasing evidence suggests the role of the gut–microbiota–brain axis in the pathogenesis of PD. Mesenchymal stem-cell-derived microvesicles (MSC-MVs) have emerged as a therapeutic potential for neurological disorders over the last years.

Objective The objective of this study was to investigate whether MSC-MVs could improve PD-like neurotoxicity in mice after administration of MPTP (1-methyl-4-phenyl-1,2,3,6-tetrahydropyridine).

Results MPTP-induced reductions in the dopamine transporter and tyrosine hydroxylase expressions in the striatum and substantia nigra (SNr) were attenuated after a subsequent single administration of MSC-MVs. Increases in the phosphorylated α -synuclein (p- α -Syn)/ α -Syn ratio in the striatum, SNr, and colon after MPTP injection were also attenuated after MSC-MVs injection. Furthermore, MSC-MVs restored MPTP-induced abnormalities of the gut microbiota composition. Interestingly, positive correlations between the genus *Dubosiella* and the p- α -Syn/ α -Syn ratio were observed in the brain and colon, suggesting their roles in the gut–microbiota–brain communication. Moreover, MSC-MVs attenuated MPTP-induced reduction of the metabolite, 3,6-dihydroxy-2-[3-methoxy-4-(sulfoxy)phenyl]-7-(sulfinooxy)-3,4-dihydro-2H-1-benzopyran-5-olate, in the blood. Interestingly, a negative correlation between this compound and the p- α -Syn/ α -Syn ratio was observed in the brain and colon.

Conclusions These data suggest that MSC-MVs could ameliorate MPTP-induced neurotoxicity in the brain and colon via the gut–microbiota–brain axis. Therefore, MSC-MVs would have a new therapeutic potential for neurological disorders such as PD.

Keywords Mesenchymal stem-cell-derived microvesicles · Gut microbiota · Metabolomics analysis · Neurotoxicity

Introduction

Parkinson’s disease (PD) is a common neurodegenerative disorder characterized by the loss of dopaminergic neurons in the substantia nigra (SNr) and striatum, accompanied by an abnormal α -synuclein (α -Syn) accumulation (Ascherio and Schwarzschild 2016; Kalia and Lang 2015). Although the precise mechanisms underlying its pathology remain unknown, accumulating evidence supports the key role of the gut microbiota in PD pathology (Klingelhoefer and Reichmann 2015; Malkki 2017; Parashar and Udayabanu 2017; Scheperjans et al. 2015; Yemula et al. 2021). Gastrointestinal dysfunction and α -Syn accumulation and activation in the enteric nervous system (ENS) always occur several years before the typical motor symptoms in patients with PD (Travagli et al. 2020). Increasing studies have demonstrated

✉ Kenji Hashimoto
hashimoto@faculty.chiba-u.jp

✉ Yi Liu
yi2006liu@163.com

¹ Department of Rheumatology and Immunology, West China Hospital, Sichuan University, Chengdu, Sichuan, China

² The Psychiatric Laboratory, The State Key Laboratory of Biotherapy, West China Hospital of Sichuan University, Chengdu, Sichuan, China

³ Division of Clinical Neuroscience, Chiba University Center for Forensic Mental Health, Chiba, Japan

that α -Syn is misfolded and deposited in the ENS and can be uploaded to the central nervous system via the vagus nerve, resulting in PD development (Holmqvist et al. 2014; Kim et al. 2019; Svensson et al. 2015). Gastrointestinal dysfunction due to dysbiosis of the gut microbiota can trigger α -Syn accumulation in the enteric nerve cells. Conversely, α -Syn accumulation also aggravated dysbiosis of the gut microbiota (Fitzgerald et al. 2019; Lei et al. 2021).

A meta-analysis of 22 studies including > 1000 patients demonstrated that the gut microbiome significantly differs between patients with PD and controls (Romano et al. 2021). Although some studies have found unaltered microbial diversity, fecal samples from patients with PD were frequently accompanied by a decreased genera *Roseburia* and *Fusicatenibacter* and increased genera *Lactobacillus* (Romano et al. 2021). MPTP (1-methyl-4-phenyl-1,2,3,6-tetrahydropyridine)-induced dopaminergic neurotoxicity is widely used as an animal model of PD (Meredith and Rademacher 2011). In 2018, Torres et al. (2018) reported that MPTP (1-methyl-4-phenyl-1,2,3,6-tetrahydropyridine) caused dopaminergic neurotoxicity in the striatum and abnormality in the diversity of gut microbiota in the wild-type mice, but not metabotropic glutamate receptor 8 (mGlu8) knock-out mice, suggesting mGluR as a novel therapeutic target for PD. Furthermore, we reported that MPTP caused altered diversity and composition of the gut microbiota (Pu et al. 2019; Shan et al. 2021). Furthermore, antibiotic-induced microbiome depletion attenuated MPTP-induced dopaminergic neurotoxicity in the mouse brain (Pu et al. 2019). Collectively, dysbiosis of gut microbiota may likely affect dopaminergic neurotoxicity in the brain of patients with PD and MPTP-treated rodents.

Mesenchymal stem-cell-derived microvesicles (MSC-MVs) are small vesicles released from the cell membrane after stress, such as hypoxia, injury, or apoptosis (Maurus et al. 2020). The MV diameter is approximately 100–1000 nm, making them the largest type of extracellular vesicles (EVs), and microvesicles (MVs) are rich in functional messenger RNAs, non-coding RNAs, proteins, lipids, DNA, and other bioactive substances (Zhang et al. 2019). MVs affect intracellular signaling pathways and exchange bioactive molecules with neighboring cells to participate in intercellular communication, cell migration, angiogenesis, and immune regulation (Dominiak et al. 2020; Jurj et al. 2020). MSC-MVs may be more advantageous than stem cells because of their small sizes, stable properties, easy storage and transportation, low immunogenicity, and low risk of tumor formation, although several limitations of MSC-MVs are addressed (Fernández-Francos et al. 2021; Matthay et al. 2017; Zhou et al. 2021). They have no ethical disputes and are highly safe. In recent years, several previous reports have used MVs for the treatment of neurodegenerative diseases such as Alzheimer's disease (AD) (Cone et al.

2021). However, no report has used MVs for the treatment of PD.

Therefore, this study aimed to evaluate whether MPTP-induced neurotoxicity in the brain and colon could be attenuated after a subsequent single treatment of MSC-MVs. Furthermore, 16S rRNA analyses for gut microbiota and metabolomic analysis of plasma metabolites were performed since several metabolites in the blood are prepared by gut microbiota.

Materials and methods

Cell culture

Standard frozen Wharton's jelly derived mesenchymal stem cells (WJ-MSCs) at passage 1 (P1) were obtained from Konjin Co., Ltd. (Chengdu, China). WJ-MSCs were isolated from postpartum umbilical cord Wharton's jelly. The maternal age was controlled at 20–32 years old, and the mother and baby were strictly screened without infectious diseases and severe genetic diseases. WJ-MSCs were negative for CD45, CD19, CD34, CD11b, and HLA-DR (all less than 2%) and positive for CD105, CD90, and CD73 (all greater than 95%) and possessed tri-lineage differentiation upon induction in vitro.

WJ-MSCs were cultured with complete culture media (CCM) composited with minimum essential medium-alpha (α -MEM, Cat# 12,571,063, Thermo Fisher Scientific, Waltham, MA), 1% penicillin/streptomycin (Cat# 15,140,122, Thermo Fisher Scientific, Waltham, MA, USA), and 10% fetal bovine plasma (FBS) (Cat# 10,091,148, Thermo Fisher Scientific, Waltham, MA, USA) on 175-mm tissue culture Petri dishes (Cat# 431,080, Corning, Corning, NY, USA) at a density of approximately 1500 cells/cm² in a standard 5% CO₂ incubator at 37 °C. The cultural media were changed every 3 days. Cells were grown to 70–80% confluence and then harvested by incubation with 0.25% trypsin/EDTA (Cat# 25,200,056, Thermo Fisher Scientific, Waltham, MA, USA) and replated for subculture up to passage 5 (P5).

Microvesicle enrichment

The P5 WJ-MSCs were washed with PBS (phosphate buffer saline) three times, the plasma-free medium was added, and the cells were starved for 48 h in a standard 5% CO₂ incubator at 37 °C. After 48 h, MSCs were rewashed with PBS, and the supernatant was collected. Then, the supernatant was centrifuged at 400 × g for 10 min and 2000 × g for 20 min at 4 °C. After centrifugation, the supernatant was transferred to a unique tube for ultracentrifugation (Avanti J-26S XP, Beckman Coulter, Brea, CA, USA) and centrifuged at

50,000 g at 4 °C for 2 h. After discarding the supernatant and washing the pellet, the mixture was centrifuged again for 2 h at 50,000 g at 4 °C. This pellet was then resuspended in sterile, filtered PBS, aliquoted, and stored at –80 °C for further analysis or diluted for intravenous administration. MVs were thawed and diluted to the correct concentration on the day of administration. Once melted, MVs were not refrozen to prevent lysis.

Nanoparticle tracking analysis

ZetaView (Twin PMX-220, Particle Metrix GmbH, Germany) was used in this experiment. After rinsing the apparatus and controlling the temperature at 24 °C, the parameters of sensitivity 70, shutter 70, min bright 20, max area 1000, and min area 5 were set. Then, 10 µl of MVs was diluted 1000 times and inspected by the apparatus.

Electron microscopy

A total of 20 µl of MV suspension was dropped onto a copper grid with carbon film for 3–5 min, and then 2% phosphotungstic acid was added to the copper grid to stain for 2 min and dry out at room temperature. The cuprum grids were observed under a transmission electron microscope (TEM: HT7800, Hitachi, Tokyo, Japan), and images were taken.

Animals

Male C57BL/6 mice (8 weeks old, 20–25 g) were purchased from HuaFuKang Co., Ltd. (Beijing, China). Mice were housed at a controlled temperature (23 ± 1 °C) and 12-h light/dark cycles (lights on between 07:00 and 19:00) with

ad libitum food (SPF mouse food; Beijing Keao Xieli Feed Co., Ltd., Beijing, China) and water. The experimental protocol of this study was approved by the Sichuan University Institutional Animal Care and Use Committee (Permission number 20211502A). The animals were deeply anesthetized with isoflurane and rapidly killed by cervical dislocation. All efforts were made to minimize mouse suffering.

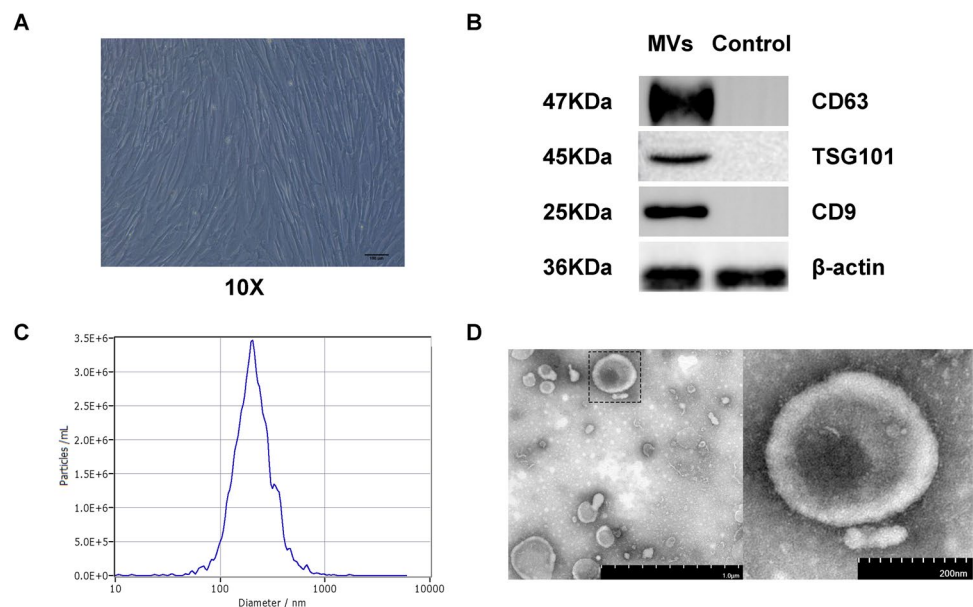
Schedule of treatment and sample collection

MPTP-induced neurotoxicity was performed as previously reported (Pu et al. 2019). Briefly, mice were randomly divided into the following four groups: saline + PBS; saline + MSC-MVs; MPTP + PBS; and MPTP + MSC-MVs. On day 1, mice received intraperitoneal injections of MPTP (10 mg/kg \times 3, 2-h interval, Tokyo Chemical Industry Co., Ltd., Tokyo, Japan) or saline (5 ml/kg \times 3, 2-h interval). One week after MPTP or saline injection, mice received MSC-MVs (5 µg/mouse) or PBS intravenously through the tail vein. On day 15, fresh fecal samples were collected and stored at –80 °C. Subsequently, mice were euthanized as described above, and plasma, colon, striatum, and substantia nigra were collected at –80 °C until use on day 15.

Western blot analysis

Western blot analysis was performed as previously reported (Pu et al. 2020, 2021; Wang et al. 2020, 2021). For MSC-MVs, 40 µl SDS-PAGE sample loading buffer (Beyotime, Shanghai, China) was added to 10 µl MSC-MVs, heated for 5 min at 95 °C, and stored at –80 °C until use. For the brain and colon tissues, the flesh was homogenized in Laemmli lysis buffer. Fifty micrograms of protein was

Fig. 1 Characteristics of WJ-MSCs and MSC-MVs. **A** Image of WJ-MSCs. Scale bar = 100 µm. **B** Immunoblot analysis of WJ-MSCs derived MVs. CD63, TSG101, and CD9 were used as biomarkers for MVs. Fibroblasts were used as control. **C** Nanoparticle tracking analysis of MSCs-MVs. **D** Electron microscopy of MSC-MVs. Scale bar = 1 µm (left) and 200 nm (right)



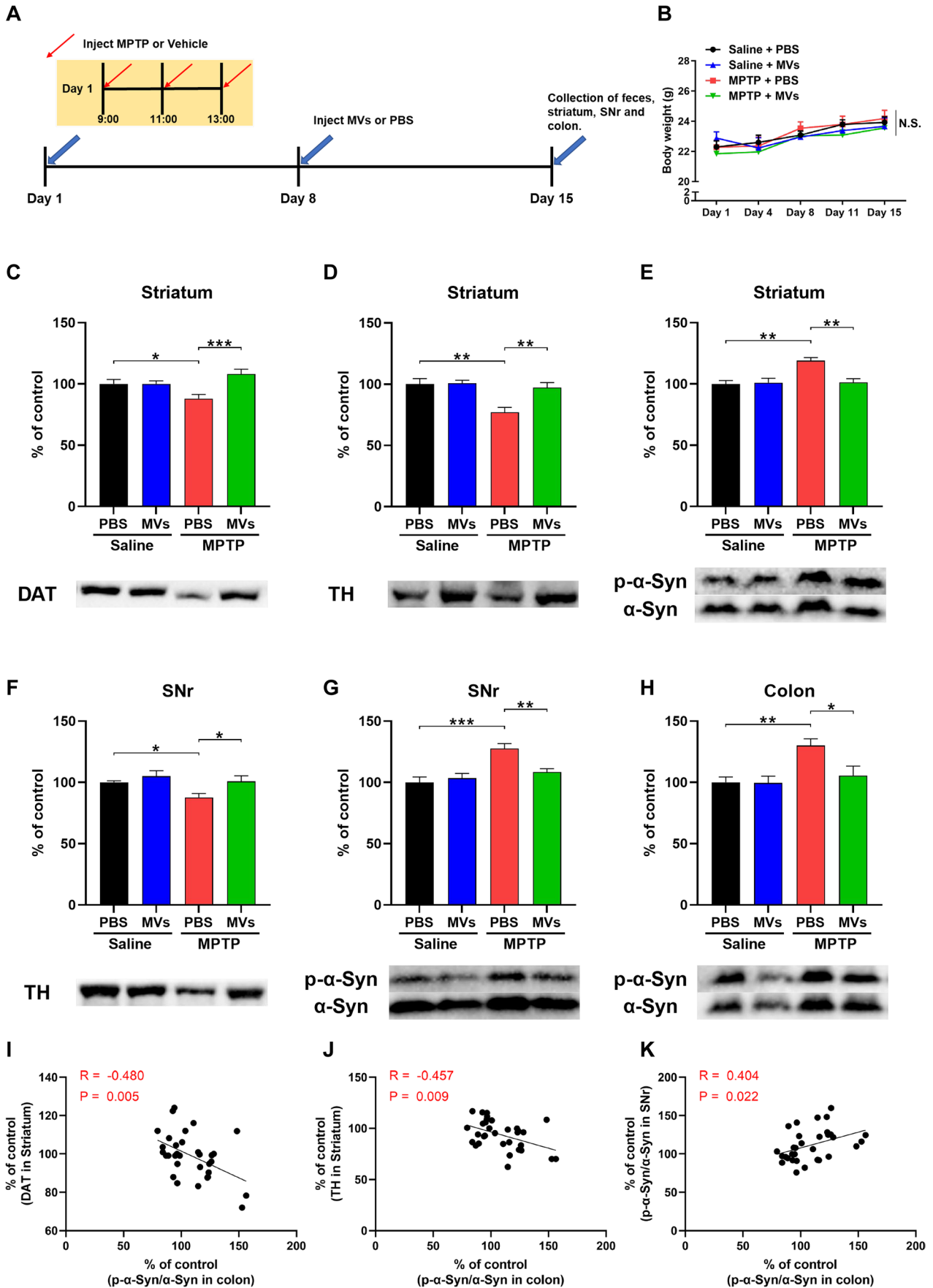


Fig. 2 Effects of MSC-MVs on MPTP-induced neurotoxicity in mice. **A** Schedule of treatment and sample collections. Mice were received saline (10 ml/kg) or MPTP (10 mg/kg) three times (at 9:00, 11:00, 13:00, i.p.) on day 1. After 7 days, mice were administered intravenously by MSC-MVs (5 µg/mouse) or vehicle (PBS). Fresh fecal samples were collected on day 15 and then the mice were sacrificed for collection of blood, brain, and colon. **B** Body weight changes among the four groups. Repeated-measures one-way ANOVA ($F_{3,28}=0.346$, $P=0.792$). **C** DAT in striatum (two-way ANOVA: MPTP: $F_{1,28}=0.307$, $P=0.5834$, MSC-MVs: $F_{1,28}=8.399$, $P=0.0072$, interaction: $F_{1,28}=8.399$, $P=0.0072$). **D** TH in striatum (two-way ANOVA: MPTP: $F_{1,28}=11.910$, $P=0.0018$, MSC-MVs: $F_{1,28}=7.445$, $P=0.0109$, interaction: $F_{1,28}=6.343$, $P=0.0178$). **E** p- α -Syn/ α -Syn ratio in striatum (two-way ANOVA: MPTP: $F_{1,28}=10.01$, $P=0.0037$, MSC-MVs: $F_{1,28}=7.550$, $P=0.104$, interaction: $F_{1,28}=9.524$, $P=0.0045$). **F** TH in the SNr (two-way ANOVA: MPTP: $F_{1,28}=5.193$, $P=0.0305$, MSC-MVs: $F_{1,28}=6.304$, $P=0.0181$, interaction: $F_{1,28}=1.239$, $P=0.2751$). **G** p- α -Syn/ α -Syn ratio in the SNr (two-way ANOVA: MPTP: $F_{1,28}=17.94$, $P=0.0002$, MSC-MVs: $F_{1,28}=4.131$, $P=0.0517$, interaction: $F_{1,28}=8.622$, $P=0.0066$). **H** p- α -Syn/ α -Syn ratio in the colon (two-way ANOVA: MPTP: $F_{1,28}=9.115$, $P=0.0054$, MSC-MVs: $F_{1,28}=4.404$, $P=0.0450$, interaction: $F_{1,28}=4.141$, $P=0.0514$). Data represent the mean \pm SEM ($n=8$). * $P<0.05$, ** $P<0.001$, *** $P<0.001$. **I** A negative correlation ($R=-0.480$, $P=0.005$) between DAT expression in the striatum and p- α -Syn/ α -Syn ratio in the colon. **J** A negative correlation ($R=-0.457$, $P=0.009$) between TH expression in the striatum and p- α -Syn/ α -Syn ratio in the colon. **K** A positive correlation ($R=0.404$, $P=0.022$) between p- α -Syn/ α -Syn ratio in the SNr and p- α -Syn/ α -Syn ratio in the colon

calculated with a BCA protein assay kit (Beyotime, Shanghai, China) and heated for 5 min at 95 °C with a quarter volume of SDS–PAGE sample loading buffer. Then, the proteins of MVs and tissue were subjected to sodium dodecyl sulfate–polyacrylamide gel electrophoresis using 10% SurePAGE gels (Cat# M00665, GenScript, Piscataway, NJ, USA). Proteins were transferred to polyvinylidene difluoride (PVDF) membranes using a Trans-Blot Mini Cell (Bio–Rad). For immunodetection, the blots were blocked with 2% BSA in TBST (TBS + 0.1% Tween-20) for 1 h at room temperature (RT) and incubated with primary antibodies against CD63 (Cat# AF5117. 1:1000, Affinity Bioscience), CD9 (Cat# AF5139. 1:1000, Affinity Bioscience), TSG101 (tumor susceptibility gene 101) (Cat# DF8427. 1:1000, Affinity Bioscience), DAT (dopamine transporter) (Cat# ab184451. 1:1000, Abcam), TH (tyrosine hydroxylase) (Cat# ab137869. 1:5000, Abcam), α -Syn (Cat# ab212184. 1:1000, Abcam), phosphorylated- α -Syn (p- α -Syn) (Cat# 51,253. 1:1000, Abcam), and β -actin (Cat# AC026. 1:100,000, ABclonal) separately at 4 °C overnight. The next day, the blots were washed three times in TBST and incubated with goat anti-rabbit IgG(H+L) (Cat# AS070. 1:10,000, ABclonal) for 1 h at room temperature. After the last three washes, the bands were detected by a Western Blotting Detection System (GE Healthcare Bioscience), and images were captured using a ChemiDoc™ Touch Imaging System (Bio–Rad Laboratories, Hercules,

CA). In this study, we used the total protein for normalization, and we did not use the protein of β -actin. The images were analyzed by Image Lab™ 3.0 software (Bio–Rad Laboratories).

16S rRNA analysis

16S rRNA analysis was performed as previously reported (Pu et al. 2020, 2021; Qu et al. 2020; Shinno-Hashimoto et al. 2021; Wang et al. 2020, 2021). DNA extraction from fecal samples was performed using a Hipure soil DNA kit (Magen, Guangzhou, China). The analysis of 16S rRNA from fecal samples was performed as previously described. Briefly, PCR was performed using 338F (5'-ACTCCTACG GGAGGCAGCAG-3') and 806R (5'-GGACTACHVGGG TWTCTAAT-3') by a thermocycler PCR system (GeneAmp 9700, ABI, USA) to amplify the V3–V4 region of the bacterial 16S rRNA gene. The amplified DNA (~330 bp) was purified using the AxyPrep DNA Gel Extraction Kit (Axygen Biosciences, Union City, CA, USA) and quantified using QuantiFluor™ ST (Promega, USA). The 16S amplicons were then sequenced using the MiSeq platform according to the Illumina protocol. Operational taxonomic units (OTUs) were clustered with a 97% similarity cutoff using UPARSE (version 7.1 <http://drive5.com/uparse/>) with a novel “greedy” algorithm that performs chimera filtering and OTU clustering simultaneously. The taxonomy of each 16S rRNA gene sequence was analyzed by the RDP classifier algorithm (<http://rdp.cme.msu.edu/>) against the Silva (SSU123) 16S rRNA database using a confidence threshold of 70%.

Plasma metabolome analysis and data preprocessing

The plasma metabolites were extracted using a 400 µl methanol to water (4:1, v/v) solution. The mixture was vortexed for 30 s and ultrasonicated at 40 kHz for 30 min at 4 °C. After centrifugation at 13,000 g at 4 °C for 15 min, the supernatant was transferred to sample vials for LC–MS analysis. An equal aliquot of each sample (10 µl) was mixed as the quality control (QC) sample. The raw data were converted into Progenesis QI 2.3 (Nonlinear Dynamics, Waters, USA) for peak detection, extraction, alignment, and integration. In total, 1016 and 2246 peaks were detected in positive and negative ionization modes, respectively. Metabolic features detected less than 80% of any set of samples, and the relative standard deviation (RSD) of QC > 30% was discarded. After that, 989 (positive mode) and 2031 (negative mode) metabolite features remained, and the remaining missing values were filled with a minimum. Then, the positive-mode and negative-mode features were concatenated for later statistical analysis.

Statistical analysis

All statistical analyses were performed using R V.4.1.3. Animal experimental data are presented as the mean ± standard error of the mean (SEM). Body weight data were analyzed using repeated one-way analysis of variance (ANOVA), followed by post hoc Tukey’s

multiple comparison tests. Western blot data were analyzed using two-way ANOVA, followed by post hoc Tukey’s multiple comparison tests. 16S rDNA data and metabolomic data were analyzed using the non-parametric Kruskal–Wallis rank-sum test, followed by Dunn’s test. *P* values of less than 0.05 were considered statistically significant.

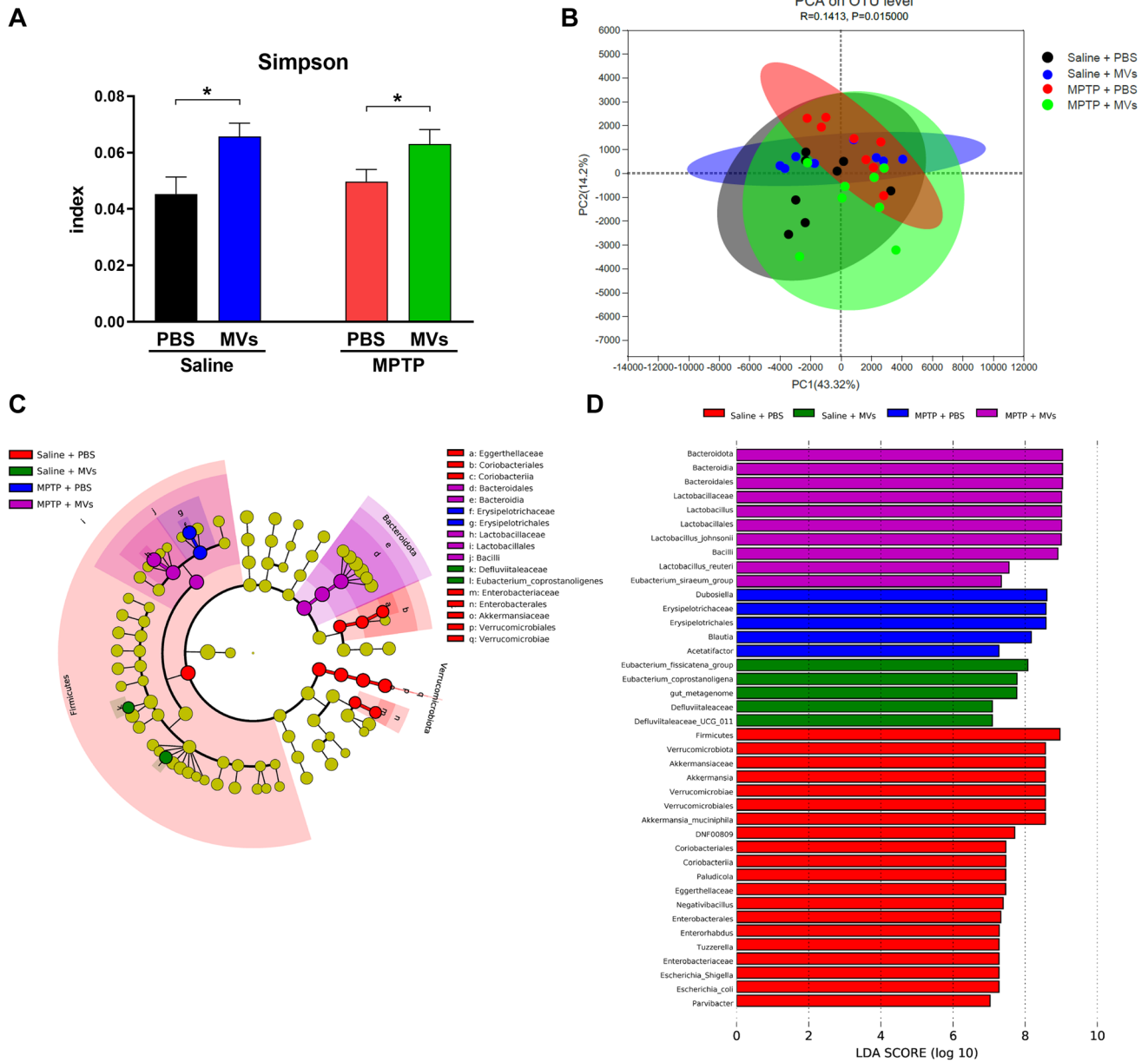


Fig. 3 Altered α -diversity and β -diversity of gut microbiota and LefSe algorithm analysis. **A** Simpson’s index of α -diversity (Kruskal–Wallis rank-sum test, $H=9.309$, $P=0.025$). **B** Principal component analysis (PCA) of β -diversity based on the OTU table, where each point represents a single sample colored by group, indicated by the second principal component of 14.2% on the Y-axis and the first principal component of 43.32% on the X-axis (ANOSIM) ($R=0.141$, $P=0.015$). **C** Cladogram (LDA score >6.0 , $P < 0.05$)

showed the taxonomic distribution difference between the four groups, indicating the different color regions. Differential abundant taxonomic clades at phylum, class, order, family, genus, and species level were shown by successive circles from the inner to outer rings. **D** Histograms of the different abundant taxa based on the cutoff value of LDA score (\log_{10}) >6.0 between the four groups. The data represent the mean ± SEM ($n=8$). $*P < 0.05$

The β diversity of unweighted UniFrac distances was analyzed. Differences in the bacterial taxa between groups at the species level or higher (depending on the taxon annotation) were calculated using linear discriminant analysis (LDA) effect size (LEfSe) with LEfSe software (Segata et al. 2011).

Metabolomic data were log₁₀ transformed and scaled to unit variance in multivariate analysis. Metabolites with (1) variable importance in the projection of > 1, (2) fold change of > 1.2 or < -0.83, and (3) $P < 0.05$ (Kruskal–Wallis rank-sum test) were regarded as differentially abundant. Orthogonal partial least square discriminant analysis (OPLS-DA) was performed in R by the ropls package. The Greipel and ggplot2 packages were used for the volcano map. The Spearman rank correlation test (psych package) was used to evaluate associations between altered taxa and metabolites among all the subjects. The heatmap package was used for the heatmap.

Results

Characterization of MSC-derived MVs

First, we cultured mesenchymal stem cells and extracted the MSC-MVs. MSC-MVs were extracted after the 175 mm cell

flasks were almost full (Fig. 1A). We performed western blot analysis to examine the expression of the proteins in MSC-MVs. Compared with fibroblasts, CD63, TSG101, and CD9 were expressed in MSC-MVs, consistent with the biomarkers of MSCs (Fig. 1B). Nanoparticle tracking analysis showed that the size of MSC-MVs was between 100 and 1000 nm, and most of the diameters were approximately 200 nm (Fig. 1C). Using TEM, we determined the size and morphology of the MVs (Fig. 1D). Collectively, these data suggested that the extracted MSC-MVs were qualified, indicating that MSC-MVs could be used for subsequent experiments.

Therapeutic effects of MSC-MVs on the neurotoxicity in the brain and colon of MPTP-treated mice

Next, we examined whether MSC-MVs could affect MPTP-induced neurotoxicity in mice. MSC-MVs were injected intravenously 7 days after MPTP injection (Fig. 2A). The body weight of the mice was not significantly changed among the four groups (Fig. 2B). Western blot analysis showed that MPTP caused reduced expression of DAT and TH in the striatum and SNr of mice although MPTP caused the increases of p- α -Syn/ α -Syn ratio in the SNr and colon

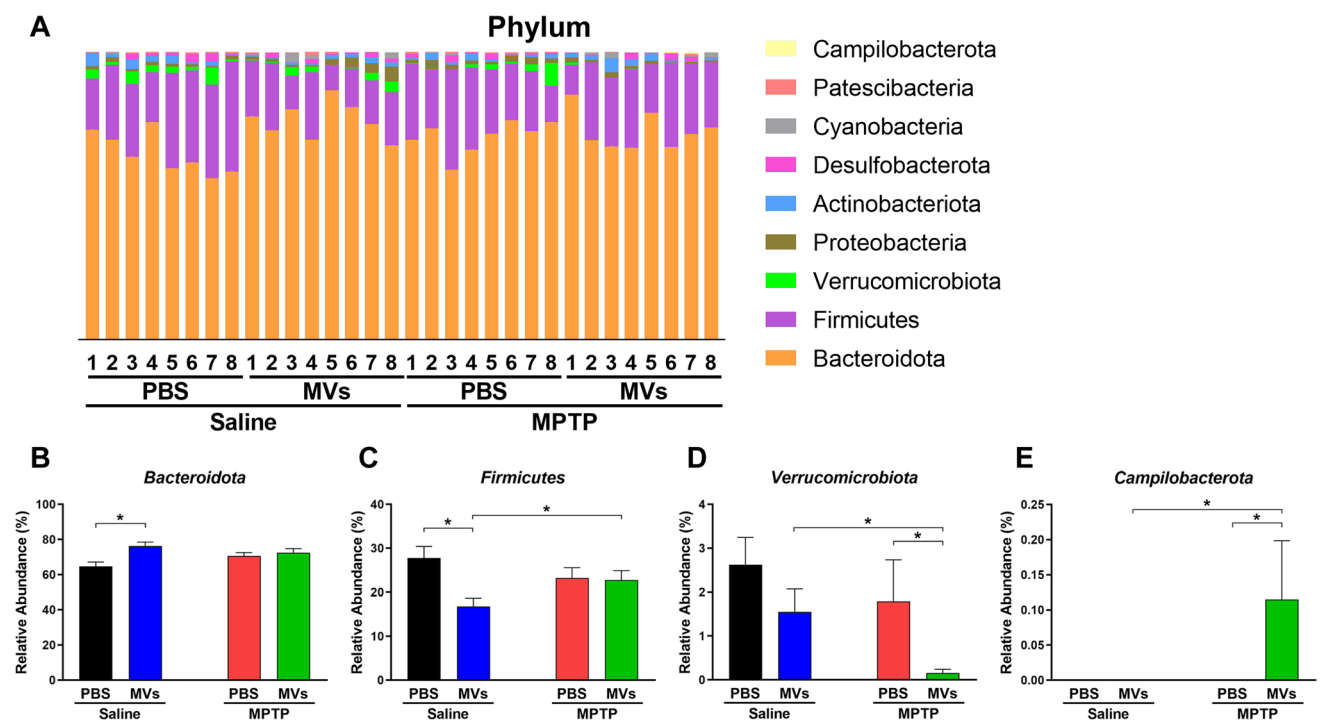
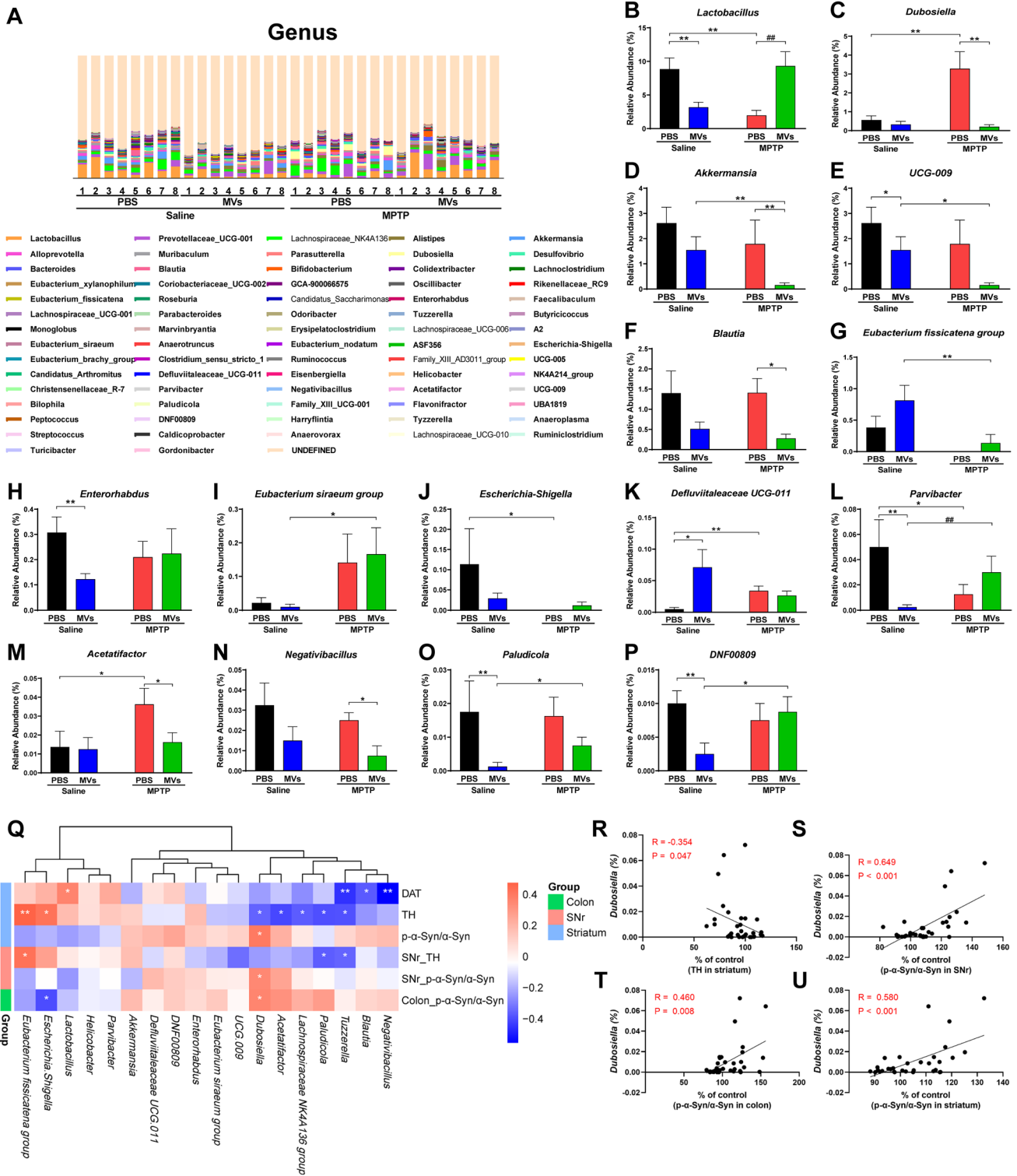


Fig. 4 Altered gut microbiota composition at phylum level. **A** Relative abundance at the phylum level. **B** *Bacteroidota* (Kruskal–Wallis rank-sum test, $H=8.315$, $P=0.040$). **C** *Firmicutes* (Kruskal–Wallis rank-sum test, $H=8.565$, $P=0.036$). **D** *Verrucomicrobiota* (Kruskal–

Wallis rank-sum test, $H=12.921$, $P=0.005$). **E** *Campilobacterota* (Kruskal–Wallis rank-sum test, $H=9.593$, $P=0.022$). The data represent the mean \pm SEM ($n=8$). * $P < 0.05$



(Fig. 2G, H). Interestingly, treatment with MSC-MVs significantly improved the altered expression of these proteins in the brain and colon by MPTP (Fig. 2C–H). These data suggest the beneficial role of MSC-MVs in the MPTP-treated mice.

Interestingly, there were negative correlations between the expression of DAT (or TH) in the striatum and the p- α -Syn/ α -Syn ratio in the colon (Fig. 2I, J). There was also a positive correlation between the p- α -Syn/ α -Syn ratio in the striatum

Fig. 5 Altered gut microbiota composition at genus level and correlation analysis. **A** Relative abundance at the genus level. **B–P** Significantly different bacteria at genus level among four groups. **B** *Lactobacillus* (Kruskal–Wallis rank-sum test, $H=16.389$, $P<0.001$). **C** *Dubosiella* (Kruskal–Wallis rank-sum test, $H=16.014$, $P=0.001$). **D** *Akkermansia* (Kruskal–Wallis rank-sum test, $H=12.921$, $P=0.005$). **E** *UCG-009* (Kruskal–Wallis rank-sum test, $H=8.489$, $P=0.037$). **F** *Blautia* (Kruskal–Wallis rank-sum test, $H=9.520$, $P=0.023$). **G** *Eubacterium fissicatena* group (Kruskal–Wallis rank-sum test, $H=13.022$, $P=0.005$). **H** *Enterorhabdus* (Kruskal–Wallis rank-sum test, $H=8.605$, $P=0.035$). **I** *Eubacterium siraeum* group (Kruskal–Wallis rank-sum test, $H=8.230$, $P=0.041$). **J** *Escherichia-Shigella* (Kruskal–Wallis rank-sum test, $H=7.931$, $P=0.047$). **K** *Defluviitaleaceae UCG-011* (Kruskal–Wallis rank-sum test, $H=10.505$, $P=0.015$). **L** *Parvibacter* (Kruskal–Wallis rank-sum test, $H=13.752$, $P=0.003$). **M** *Acetatifactor* (Kruskal–Wallis rank-sum test, $H=8.356$, $P=0.039$). **N** *Negativibacillus* (Kruskal–Wallis rank-sum test, $H=8.814$, $P=0.032$). **O** *Paludicola* (Kruskal–Wallis rank-sum test, $H=10.819$, $P=0.013$). **P** *DNF00809* (Kruskal–Wallis rank-sum test, $H=8.147$, $P=0.043$). **Q** The heatmap depicts relationships between the genus taxa and proteins. **R–U** Examples of individual taxa–proteins associations. Data represent the mean \pm SEM. ($n=8$). * $P<0.05$, ** $P<0.001$, *** $P<0.001$

and the p- α -Syn/ α -Syn ratio in the colon (Fig. 2K). These data suggest a link between the brain and the colon.

Effects of MPTP and MSC-MVs on gut microbiota composition

We performed 16S ribosome RNA sequencing analysis of the fecal samples. For α diversity, the Simpson index of

both saline and MPTP groups was significantly increased after MSC-MVs treatment (Fig. 3A), although other indices (Chao1, Shannon, ACE) were not altered after the treatments (data not shown). Principal component analysis (PCA) showed a remarkable difference in microbiota composition among the four groups (Fig. 3B).

Next, we used LEfSe algorithm analysis for high-dimensional biomarker discovery among the four groups by the raw data from the OTU table. Different colors represent different abundant taxa and different microbial biomarkers. The classification of potential microbial markers between the four groups is presented (Fig. 3C). Five mixed-level phylotypes, including *Dubosiella*, *Erysipelotrichaceae*, *Erysipelotrichales*, *Blautia*, and *Acetatifactor*, were identified as potential microbial markers in the MPTP-treated group (Fig. 3D). Additionally, ten mixed-level phylotypes, including *Bacteroidota*, *Bacteroidia*, *Bacteroidales*, *Lactobacillus*, *Lactobacillales*, *Lactobacillus johnsonii*, *Bacilli*, *Lactobacillus reuteri*, and *Eubacterium siraeum* group, were identified as potential microbial markers in the MPTP + MVs-treated group (Fig. 3D).

Furthermore, the relative abundance was used to define differential bacteria between the four groups at three different levels. Four significantly different phyla were identified (e.g., *Bacteroidota*, *Firmicutes*, *Verrucomicrobiota*, *Compiobacterota*) (Fig. 4). At the genus level, the abundance of fifteen genera (*Lactobacillus*, *Dubosiella*, *Akkermansia*, etc.) was significantly different between the four groups

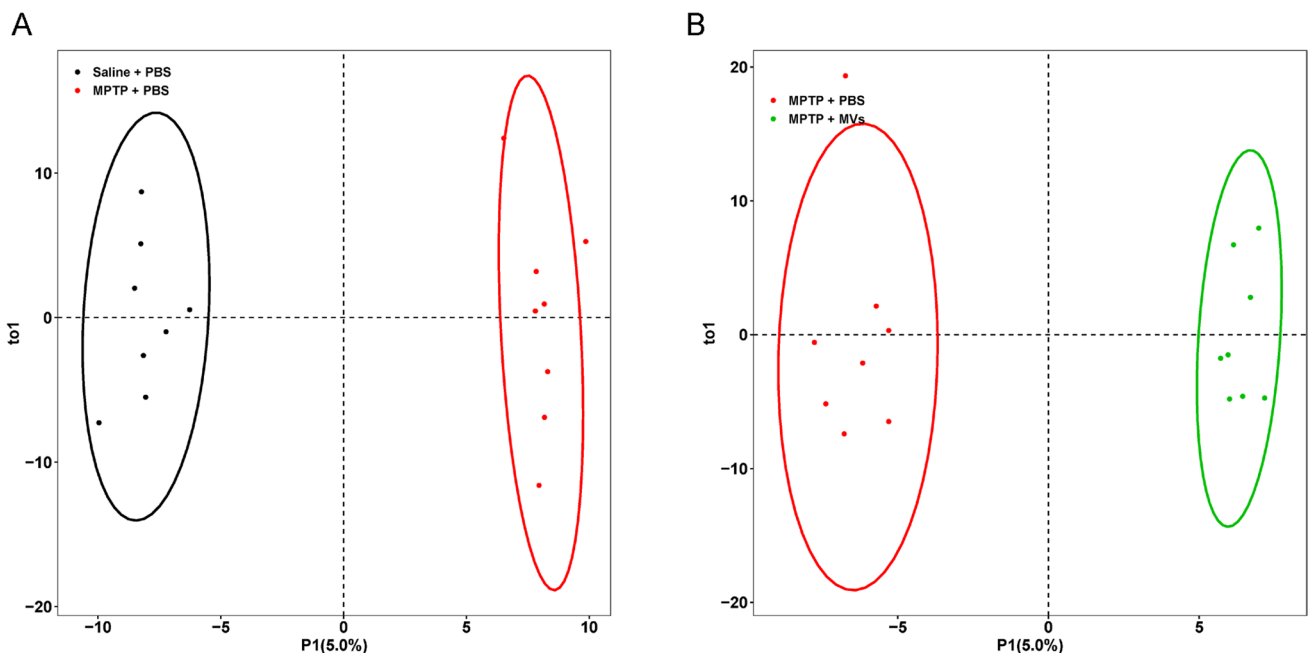


Fig. 6 Orthogonal partial least squares discriminant analysis of plasma metabolites. **A** OPLS-DA between control group and MPTP + PBS group. **B** OPLS-DA between MPTP + PBS group and MPTP + MSC-MVs group

(Fig. 5A–P). *Dubosiella* and *Acetatifactor* were significantly increased in MPTP-treated mice, and MSC-MVs treatment attenuated MPTP-induced increases of these bacteria. We performed a correlation analysis between genera and the expression of proteins (Fig. 5Q). The relative abundance of several bacteria such as *Tuzzerella* negatively correlated with the expression of DAT and TH in the brain. Interestingly, the relative abundance of *Dubosiella* was positively correlated with the p- α -Syn/ α -Syn ratio in the brain and colon, and negatively correlated with TH in the striatum (Fig. 5R–U).

Effects of MPTP and MSC-MVs on plasma metabolomics

We performed untargeted metabolomics analysis on plasma samples since the gut microbiota affects metabolites in the blood. After alignment with the database, 479 metabolites were accurately identified. Similar to PCA, OPLS-DA was used to analyze the overall distribution of metabolites. OPLS-DA revealed that the metabolic composition of the MPTP+PBS group significantly deviated from controls as

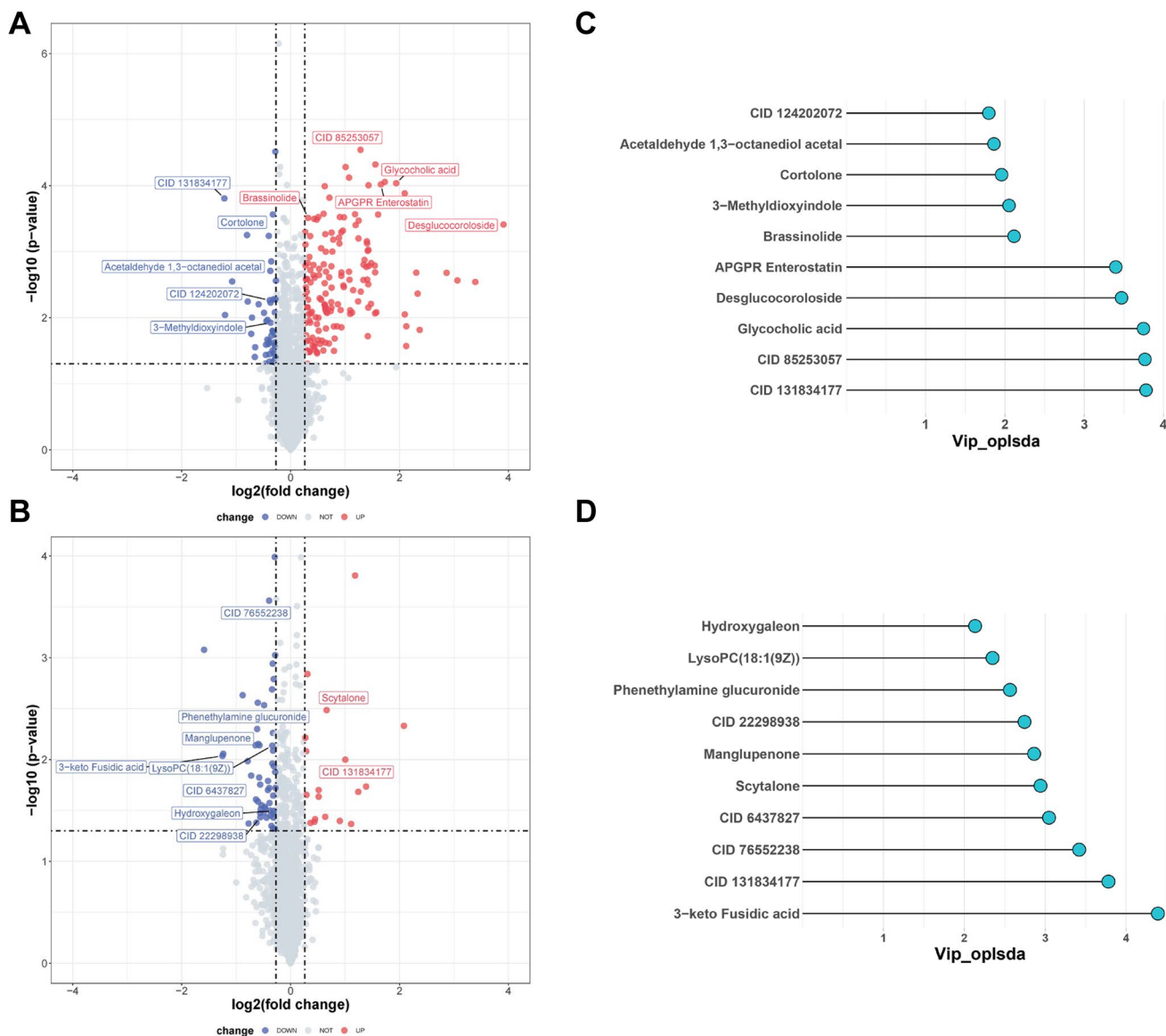


Fig. 7 Altered plasma metabolites after MPTP and MSC-MVs treatment. **A** Volcano plot demonstrated metabolites changes in MPTP-treated mice ($n=41$) compared with control mice. **B** Volcano plot showed metabolites changes in MPTP+MSC-MVs group ($n=15$) compared with MPTP+PBS group. The X-axis indicates \log_2 -transformed FC of plasma metabolites abundances, and Y-axis denotes $-\log_{10}$ -transformed P value analyzed using the Kruskal–

Wallis rank-sum test. The horizontal lines represent $P < 0.05$ and vertical lines indicate FC of > 1.2 or < -0.83 . Metabolites elevated or decreased are highlighted in red and blue, respectively, and metabolites with the highest VIP and lowest P are labeled with text. **C**, **D** Lollipop chart visualized the VIP index calculated by OPLS-DA of the labeled metabolites named in **A** and **B** separately

well as from MPTP + MSC-MVs group (Fig. 6A, B), suggesting dramatic changes in plasma metabolites after the MPTP and MSC-MVs treatments.

Next, we analyzed the different metabolites between the four groups. Compared with the control, 7 metabolites were significantly decreased and 34 metabolites were significantly increased in MPTP-treated mice (Fig. 7A and Table S1). Furthermore, compared with MPTP + PBS group, 2 metabolites were significantly increased and 13 metabolites decreased in the MPTP + MSC-MVs group (Fig. 7B and Table S2). PubChem CID numbers were used instead of names when the structures of the compounds were complex (<https://pubchem.ncbi.nlm.nih.gov>). See Table S3 for the converted CID numbers. In addition, metabolites with the highest VIP (variable important in projection) and lowest *P* values were exhibited (Fig. 7C, D). Interestingly, we found that MPTP significantly reduced CID 131,834,177 (3,6-dihydroxy-2-[3-methoxy-4-(sulfooxy)phenyl]-7-(sulfinooxy)-3,4-dihydro-2H-1-benzopyran-5-olate) in the plasma of mice, although MSC-MVs restored MPTP-induced reduction of the metabolite.

Associations between altered microbiota, blood metabolites, and proteins

Considering the interplay between the gut microbiome and blood metabolites, we performed correlation analysis to examine the associations between the differentially abundant genera and blood metabolites (Fig. 8A). We found that the abundance of gut microbiota is associated with blood metabolites, and one genus often affects multiple metabolites. Most of the differential metabolites (e.g., cholic acid, Delta2-THA, nutriacholic acid) were negatively correlated with *Lactobacillus* and *DNF00809*. Additionally, *Blautia* and *Negativibacillus* were positively correlated with the other metabolites (e.g., cortolone and hydroxygaleon).

To further understand whether taxa and metabolites contribute to MPTP-induced neurotoxicity, we tested for their correlations with western blot results using the Spearman correlation (Fig. 8B). The metabolite CID 131,834,177 was significantly negatively correlated with the p- α -Syn/ α -Syn ratio in both the brain and colon and it was positively correlated with TH expression in the striatum (Fig. 8C–F). In addition to *Tuzzerella* and *Dubosiella*, the genera *Eubacterium fissicatena* group, *Paludicola*, *Escherichia-Shigella*, and the compound LysoPC (18:1(9Z)) showed multiple correlations with the expression of proteins.

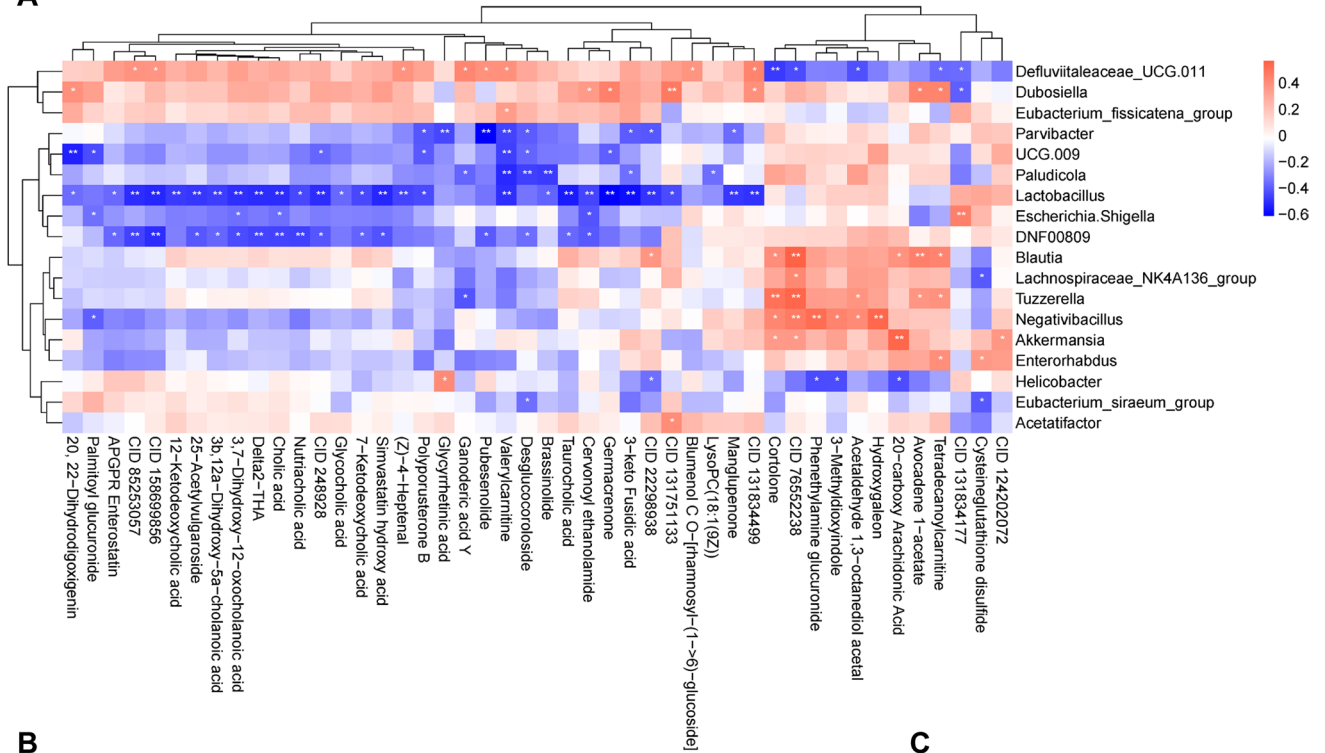
Discussion

The major findings of this study are as follows. First, MPTP-induced reduction in DAT and TH in the striatum and SNr, and increased p- α -Syn/ α -Syn ratio in the striatum, SNr,

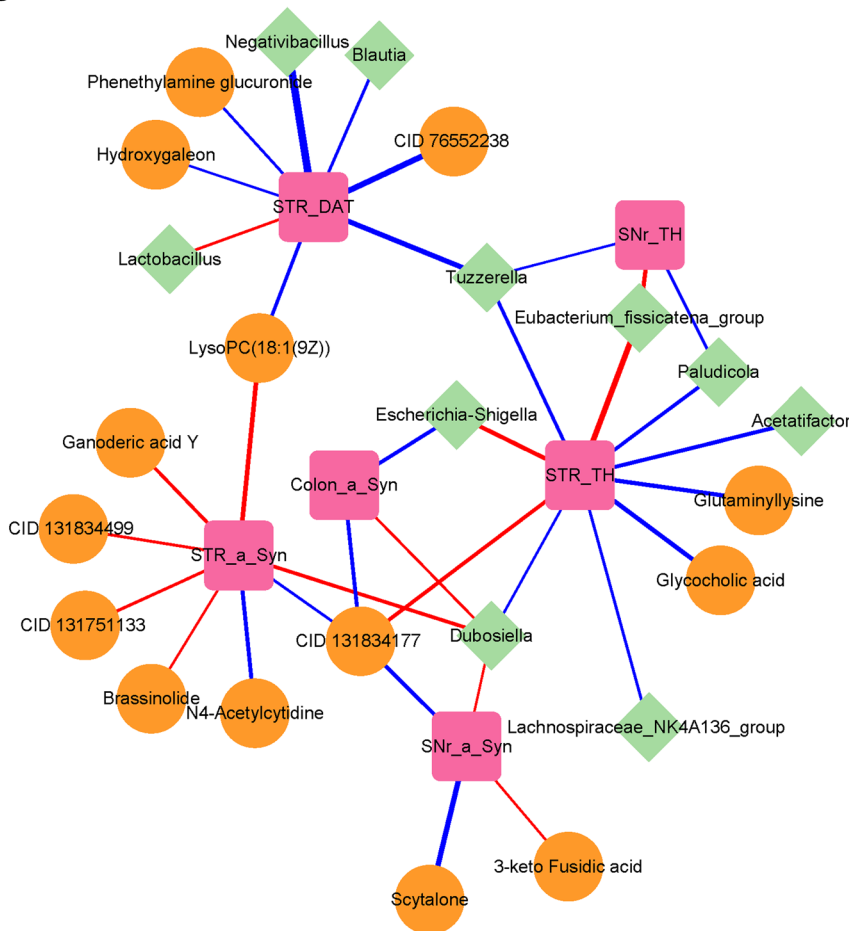
and colon were significantly ameliorated after a subsequent single intravenous administration of MSC-MVs. Second, MSC-MVs improved the abnormal β -diversity of the gut microbiota caused by MPTP injection. The LEfSe algorithm identified five and ten mix-level taxa as specific microbial biomarkers in the MPTP + PBS and MPTP + MSC-MVs groups, respectively. In particular, the relative abundance of the genera *Dubosiella* and *Acetatifactor* was significantly higher in the MPTP + PBS group, and MSC-MVs significantly attenuated MPTP-induced increases of these bacteria. Furthermore, *Dubosiella* was positively correlated with α -Syn phosphorylation in the brain and colon, whereas *Dubosiella* (or *Acetatifactor*) was negatively correlated with TH expression in the brain. These results suggest that *Dubosiella* and *Acetatifactor* may play a role in the beneficial effects of MSC-MVs in MPTP-treated mice. Third, metabolomic analysis suggests that several metabolites such as CID 131,834,177 may affect MPTP-induced toxicity and beneficial effects of MSC-MVs. Finally, CID 131,834,177 was negatively correlated with the p- α -Syn/ α -Syn ratio in the striatum, SNr, and colon. Taken together, MSC-MVs could treat MPTP-induced neurotoxicity in the brain and colon by regulating the gut–microbiota–brain axis including microbiome-derived metabolites.

Stem cells have been used for the treatment of neurodegenerative disorders, such as AD, multiple sclerosis, and PD, for the last 20 years (Sakthiswary and Raymond 2012). Clinical studies have shown that scale scores and subjective feelings of patients with PD significantly improved after stem cell therapies (Venkataramana et al. 2012). Recently, Park et al. reported that injection of human adipose-derived stem cells restored the altered DAT expression and abnormal motor function in MPTP-treated mice (Park and Chang 2020). However, due to cellular activity and tumorigenicity, the use of stem cells for disease treatment has very slowly developed in recent years (Gordeeva and Khaydukov 2017). In this case, stem-cell-derived EVs were found to be strongly effective therapeutically and highly safe and have been extensively investigated for the treatment of various neurological diseases. In a study of AD, EV injection reduced the production and deposition of amyloid- β peptides in amyloid precursor protein transgenic mice (Dinkins et al. 2017). Furthermore, EVs decreased behavioral scores and demyelination in experimental autoimmune encephalomyelitis mice, an animal model of MS (Li et al. 2019). In this study, MSC-MVs were found to ameliorate the reduction of DAT and TH expressions in the striatum and SNr of MPTP-treated mice, consistent with those of a previous report using exosomes (Chen et al. 2020). Moreover, MSC-MVs were also found to attenuate the MPTP-induced increase of the α -Syn/ α -Syn ratio in the brain and colon. Remarkably, a single injection of MSC-MVs 7 days after MPTP injection could improve MPTP-induced neurotoxicity in the brain and colon, indicating a potent therapeutic effect of MSC-MVs. Precise mechanisms of MSC-MVs' therapeutic effects

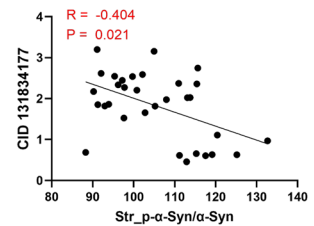
A



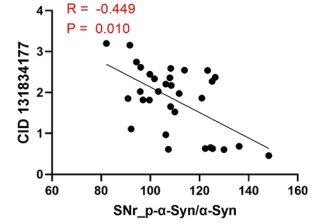
B



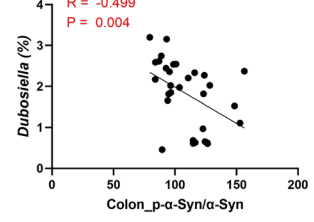
C



D



E



F

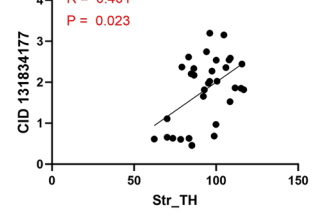


Fig. 8 Correlation analysis among microbiota, metabolites, and proteins. **A** The heatmap depicted the relationships between the taxa and metabolites changed in MPTP+PBS group and MPTP+MSC-MVs group. **B** Integrative network revealed associations between differentially abundant taxa or metabolites and expression of proteins. **C–F** Examples of CID 131,834,177 and protein associations

are currently unclear. Previous reports suggested that abnormal α -Syn phosphorylation occurs in the gut earlier than that in the brain (Li et al. 2019; Shannon et al. 2012). Interestingly, the TH expression in the striatum was negatively correlated with p- α -Syn/ α -Syn expression in the colon, suggesting a role of gut–brain communication (Shan et al. 2021). Collectively, it is likely that MSC-MVs may, in part, alleviate MPTP-induced neurotoxicity by reducing the accumulation and transportation of α -Syn in the colon, although further study is needed.

We previously reported that antibiotic-induced microbiome depletion protected against MPTP-induced dopaminergic neurotoxicity in the mouse brain, suggesting its role in MPTP-induced neurotoxicity in the brain (Pu et al. 2019). In this study, MSC-MVs were found to improve the abnormal composition of gut microbiota of MPTP-treated mice, suggesting a beneficial role of MSC-MVs in regulating gut microbiota in the intestine. Given the essential roles of MVs in intracellular communications (Zhang et al. 2019), intracellular communications of MSC-MVs might play a role in its therapeutic effects in the MPTP model through the potent anti-inflammatory and neuroprotective effects.

The LEfSe algorithm identified *Dubosiella* and *Acetatifactor* as specific microbial biomarkers for the MPTP-treated group. Interestingly, the relative abundance of *Dubosiella* and *Acetatifactor* was significantly increased after the MPTP treatment, and MSC-MVs restored the increased abundance of these bacteria in the MPTP-treated mice. Furthermore, *Dubosiella* was elevated in fecal samples of dextran sulfate sodium-induced colitis mice, suggesting an inflammatory role of *Dubosiella* (Li et al. 2022). *Dubosiella* has been reportedly elevated in the feces of mice with chronic stress-induced depression compared with the control mice (Westfall et al. 2021). A recent study showed that *Acetatifactor* was associated with increased freezing time in fear-conditioning training in MPTP-treated mice (Torres et al. 2018). Furthermore, *Dubosiella* and *Acetatifactor* were positively correlated with the p- α -Syn/ α -Syn ratio in the brain or gut. Moreover, the relative abundance of the two genera was found to be negatively correlated with TH expression in the striatum. Given the inflammatory role of *Dubosiella* and *Acetatifactor*, the augmentation of these two genera in the intestine might be associated with the beneficial effects of MSC-MVs on the MPTP-induced increase of the p- α -Syn/ α -Syn ratio in the colon. However, it is unclear how a single MSC-MV injection can restore an abnormal composition of these two bacteria in

MPTP-treated mice. Further study is needed to confirm the role of these two bacteria in the beneficial effects of MSC-MVs in the MPTP model.

Using metabolomics analysis, 3,6-dihydroxy-2-[3-methoxy-4-(sulfooxy)phenyl]-7-(sulfinooxy)-3,4-dihydro-2H-1-benzopyran-5-olate (CID 131,834,177) levels were found to be significantly decreased in the MPTP-treated mice, whereas the metabolite was restored by injecting MSC-MVs. Interestingly, CID 131,834,177 was negatively correlated with the p- α -Syn/ α -Syn ratio in the striatum, SNr, and colon, whereas the concentration of this metabolite was positively correlated with TH expression in the striatum. CID 131,834,177 is one of the catechins. Catechins are a class of polyphenolic compounds that primarily occur in many plants, and all have strong pharmacological properties that influence the host metabolism and immunity, including neuroprotective, anti-inflammatory, and cardioprotective properties (Blagojević et al. 2021; Ding et al. 2020; Soares et al. 2020). Catechins are mainly divided into epicatechin (EC), epigallocatechin (EGC), epicatechin gallate (ECG), and epigallocatechin gallate (EGCG). A recent study showed that ECG could attenuate rotenone-induced degeneration of dopaminergic neurons in the SHSY5Y cells, a common cell model of PD (Luo et al. 2021). Furthermore, EGCG prevented MPTP-induced dopamine depletion and loss of dopaminergic neurons in the striatum (Bitu Pinto et al. 2015). Moreover, catechin improved motor performance and dopaminergic neuron functions in PD model rats induced by unilateral striatal injection of 6-hydroxydopamine (Teixeira et al. 2013). Based on the solid neuroprotective effects of catechins, reduced CID 131,834,177 levels in the blood may play a role in the neurotoxicity of MPTP-treated mice. Interestingly, the relative abundance of *Dubosiella* strongly negatively correlated with the CID 131,834,177 concentration, suggesting that *Dubosiella* may affect the CID 131,834,177 production in the intestine. Therefore, whether *Dubosiella* and CID 131,834,177 are altered in patients with PD should be investigated.

The present study showed that MVs attenuated MPTP-induced increases in metabolite concentrations, including 3-keto fusidic acid, LysoPC(18:1(9Z)), blumenol CO-[rhamnosyl-(1->6)-glucoside], and manglupenone. Fusidic acid is a topical antibiotic frequently used to treat skin infections, especially for gram-positive bacteria (Bonamonte et al. 2014). LysoPC(18:1(9Z)) levels are thought to be commonly associated with energy metabolisms, such as obesity and hyperlipidemia (Zhong et al. 2013). LysoPC(18:1(9Z)) was increased in obese mice and those fed a high-fat diet (Cai et al. 2021). Interestingly, the fusidic acid (or LysoPC) concentration was found to be positively collated with the α -Syn expression, suggesting a role of these metabolites in α -Syn-related toxicity. Manglupenone is a

triterpenoid. Triterpenoids are reported to attenuate dopaminergic neurotoxicity in MPTP-treated mice (Kaidery et al. 2013). Collectively, these metabolites may play a role in the effects of MPTP-induced neurotoxicity and therapeutic effects of MVs. Nonetheless, further research is needed to clarify the roles of these metabolites in PD.

Beneficial effects of multipotential bone marrow stromal cells on brain functions have been reported (Boxall and Jones 2012; Phinney and Prokop 2007; Soliman et al. 2021). For example, intracerebral injection of bone marrow stromal cells into Apoe knock-out mice caused enhanced novel object recognition and increased microtubule-associated protein in the dentate gyrus of the hippocampus, suggesting their therapeutic potential for neurodegenerative disorders (Peister et al. 2006). Collectively, multipotential bone marrow stromal cells are vital for the development, maintenance, function, and regeneration of most tissues including the brain (Soliman et al. 2021).

In summary, the present study shows that intravenous injection of MSC-MVs could improve MPTP-induced neurotoxicity in the striatum and colon through the gut–microbiota–brain axis. Therefore, intravenous injection of MSC-MVs could likely be a new therapeutic approach for neurodegenerative disorders such as PD.

Supplementary Information The online version contains supplementary material available at <https://doi.org/10.1007/s00213-023-06348-0>.

Author contributions Y.P., K.H., and Y.L. contributed to conception and design of the study. Y.P., Q.W., Q.Z., T.H., J.W., and L.W. contributed to acquisition and analysis of data. Y.P. contributed to drafting the text or preparing the figures. Y.L. supervised the project. All authors approved the final version of the text.

Funding This study was supported by the National Natural Science Foundation of China (to Y. Pu, no. 82101616), the China Postdoctoral Science Foundation (to Y. Pu, no. 281269), the Post-Doctor Research Project, West China Hospital, Sichuan University (to Y. Pu, no. 2021HXBH046), and the 1-3-5 project for disciplines of excellence, West China Hospital, Sichuan University (to Y. Liu, nos. ZYGD18015 and ZYJC18003).

Data availability The 16S rRNA sequencing data have been deposited to the NCBI Sequence Read Archive and are available at the accession number PRJNA833302.

Declarations

Conflict of interest The authors declare no competing interests.

References

- Ascherio A, Schwarzschild MA (2016) The epidemiology of Parkinson's disease: risk factors and prevention. *Lancet Neurol* 15:1257–1272
- Bitu Pinto N, da Silva Alexandre B, Neves KR, Silva AH, Leal LK, Viana GS (2015) Neuroprotective properties of the standardized extract from *Camellia sinensis* (green tea) and its main bioactive components, epicatechin and epigallocatechin gallate, in the 6-OHDA model of Parkinson's disease. *Evid Based Complement Alternat Med* 2015:161092
- Blagojević B, Agić D, Serra AT, Matic S, Matovina M, Bijelić S, Popović BM (2021) An in vitro and in silico evaluation of bioactive potential of cornelian cherry (*Cornus mas* L) extracts rich in polyphenols and iridoids. *Food Chem* 335:127619
- Bonamonte D, Belloni Fortina A, Neri L, Patrizi A (2014) Fusidic acid in skin infections and infected atopic eczema. *G Ital Dermatol Venereol* 149:453–459
- Boxall SA, Jones E (2012) Markers for characterization of bone marrow multipotential stromal cells. *Stem Cells Int* 2012:975871
- Cai H, Wen Z, Meng K, Yang P (2021) Metabolomic signatures for liver tissue and cecum contents in high-fat diet-induced obese mice based on UHPLC-Q-TOF/MS. *Nutr Metab (lond)* 18:69–69
- Chen H-X, Liang F-C, Gu P, Xu B-L, Xu H-J, Wang W-T, Hou J-Y, Xie D-X, Chai X-Q, An S-J (2020) Exosomes derived from mesenchymal stem cells repair a Parkinson's disease model by inducing autophagy. *Cell Death Dis* 11:288
- Cone AS, Yuan X, Sun L, Duke LC, Vreones MP, Carrier AN, Kenyon SM, Carver SR, Bentham SD, Stimmell AC, Moseley SC, Hike D, Grant SC, Wilber AA, Olcese JM, Meckes DG Jr (2021) Mesenchymal stem cell-derived extracellular vesicles ameliorate Alzheimer's disease-like phenotypes in a preclinical mouse model. *Theranostics* 11:8129–8142
- Ding T, Cao K, Fang W, Zhu G, Chen C, Wang X, Wang L (2020) Evaluation of phenolic components (anthocyanins, flavanols, phenolic acids, and flavonols) and their antioxidant properties of peach fruits. *Sci Hortic* 268:109365
- Dinkins MB, Wang G, Bieberich E (2017) Sphingolipid-enriched extracellular vesicles and Alzheimer's disease: a decade of research. *J Alzheimers Dis* 60:757–768
- Dominiak A, Chelstowska B, Olejarz W, Nowicka G (2020) Communication in the cancer microenvironment as a target for therapeutic interventions. *Cancers (basel)* 12:1232
- Fernández-Francos S, Eiro N, González-Galiano N, Vizoso FJ (2021) Mesenchymal stem cell-based therapy as an alternative to the treatment of acute respiratory distress syndrome: current evidence and future perspectives. *Int J Mol Sci* 22(15):7850
- Fitzgerald E, Murphy S, Martinson HA (2019) Alpha-synuclein pathology and the role of the microbiota in Parkinson's disease. *Front Neurosci* 13:369–369
- Gordeeva O, Khaydukov S (2017) Tumorigenic and differentiation potentials of embryonic stem cells depend on TGFβ family signaling: lessons from teratocarcinoma cells stimulated to differentiate with retinoic acid. *Stem Cells Int* 2017:7284872–7284872
- Holmqvist S, Chutna O, Bousset L, Aldrin-Kirk P, Li W, Björklund T, Wang ZY, Roybon L, Melki R, Li JY (2014) Direct evidence of Parkinson pathology spread from the gastrointestinal tract to the brain in rats. *Acta Neuropathol* 128:805–820
- Jurj A, Zanoaga O, Braicu C, Lazar V, Tomuleasa C, Irimie A, Berindan-Neagoe I (2020) A comprehensive picture of extracellular vesicles and their contents. *Molecular Transfer to Cancer. Cells Cancers (basel)* 12:298
- Kaidery NA, Banerjee R, Yang L, Smirnova NA, Hushpulia DM, Liby KT, Williams CR, Yamamoto M, Kensler TW, Ratan RR, Sporn MB, Beal MF, Gazaryan IG, Thomas B (2013) Targeting Nrf2-mediated gene transcription by extremely potent synthetic triterpenoids attenuate dopaminergic neurotoxicity in the MPTP mouse model of Parkinson's disease. *Antioxid Redox Signal* 18:139–157
- Kalia LV, Lang AE (2015) Parkinson's disease. *Lancet* 386:896–912
- Kim S, Kwon SH, Kam TI, Panicker N, Karuppagounder SS, Lee S, Lee JH, Kim WR, Kook M, Foss CA, Shen C, Lee H, Kulkarni S, Pasricha PJ, Lee G, Pomper MG, Dawson VL, Dawson TM, Ko HS (2019) Transneuronal propagation of pathologic

- α -synuclein from the gut to the brain models Parkinson's disease. *Neuron* 103:627–641.e627
- Klingelhoefer L, Reichmann H (2015) Pathogenesis of Parkinson disease—the gut–brain axis and environmental factors. *Nat Rev Neurol* 11:625–636
- Lei Q, Wu T, Wu J, Hu X, Guan Y, Wang Y, Yan J, Shi G (2021) Roles of α -synuclein in gastrointestinal microbiome dysbiosis-related Parkinson's disease progression (Review). *Mol Med Rep* 24:734
- Li Z, Liu F, He X, Yang X, Shan F, Feng J (2019) Exosomes derived from mesenchymal stem cells attenuate inflammation and demyelination of the central nervous system in EAE rats by regulating the polarization of microglia. *Int Immunopharmacol* 67:268–280
- Li Q, Chen G, Zhu D, Zhang W, Qi S, Xue X, Wang K, Wu L (2022) Effects of dietary phosphatidylcholine and sphingomyelin on DSS-induced colitis by regulating metabolism and gut microbiota in mice. *J Nutr Biochem* 105:109004
- Luo S, Sun X, Huang M, Ma Q, Du L, Cui Y (2021) Enhanced neuroprotective effects of epicatechin gallate encapsulated by bovine milk-derived exosomes against Parkinson's disease through antiapoptosis and antimetaphagy. *J Agric Food Chem* 69:5134–5143
- Malkki H (2017) Could gut microbiota influence severity of Parkinson disease? *Nat Rev Neurol* 13:66–67
- Matthay MA, Pati S, Lee JW (2017) Concise review: mesenchymal stem (stromal) cells: biology and preclinical evidence for therapeutic potential for organ dysfunction following trauma or sepsis. *Stem Cells* 35:316–324
- Maumus M, Rozier P, Boulestreau J, Jorgensen C, Noël D (2020) Mesenchymal stem cell-derived extracellular vesicles: opportunities and challenges for clinical translation. *Front Bioeng Biotechnol* 8:997–997
- Meredith GE, Rademacher DJ (2011) MPTP mouse models of Parkinson's disease: an update. *J Parkinson Dis* 1:19–33
- Parashar A, Udayabanu M (2017) Gut microbiota: implications in Parkinson's disease. *Parkinsonism Relat Disord* 38:1–7
- Park H, Chang KA (2020) Therapeutic potential of repeated intravenous transplantation of human adipose-derived stem cells in subchronic MPTP-induced Parkinson's disease mouse model. *Int J Mol Sci* 21:8129
- Peister A, Zeitouni S, Pfankuch T, Reger RL, Prockop DJ, Raber J (2006) Novel object recognition in *ApoE*^{-/-} mice improved by neonatal implantation of wild-type multipotential stromal cells. *Exp Neurol* 201:266–269
- Phinney DG, Prockop DJ (2007) Concise review: mesenchymal stem/multipotent stromal cells: the state of transdifferentiation and modes of tissue repair—current views. *Stem Cells* 25:2896–2902
- Pu Y, Chang L, Qu Y, Wang S, Zhang K, Hashimoto K (2019) Antibiotic-induced microbiome depletion protects against MPTP-induced dopaminergic neurotoxicity in the brain. *Aging (Albany NY)* 11:6915–6929
- Pu Y, Yang J, Chang L, Qu Y, Wang S, Zhang K, Xiong Z, Zhang J, Tan Y, Wang X, Fujita Y, Ishima T, Wang D, Hwang SH, Hammock BD, Hashimoto K (2020) Maternal glyphosate exposure causes autism-like behaviors in offspring through increased expression of soluble epoxide hydrolase. *Proc Natl Acad Sci U S A* 117:11753–11759
- Pu Y, Tan Y, Qu Y, Chang L, Wang S, Wei Y, Wang X, Hashimoto K (2021) A role of the subdiaphragmatic vagus nerve in depression-like phenotypes in mice after fecal microbiota transplantation from *Chrna7* knock-out mice with depression-like phenotypes. *Brain Behav Immun* 94:318–326
- Qu Y, Zhang K, Pu Y, Chang L, Wang S, Tan Y, Wang X, Zhang J, Ohnishi T, Yoshikawa T, Hashimoto K (2020) Betaine supplementation is associated with the resilience in mice after chronic social defeat stress: a role of brain–gut–microbiota axis. *J Affect Disord* 272:66–76
- Romano S, Savva GM, Bedarf JR, Charles IG, Hildebrand F, Narbad A (2021) Meta-analysis of the Parkinson's disease gut microbiome suggests alterations linked to intestinal inflammation. *npj Parkinson's Dis* 7:27
- Sakthiswary R, Raymond AA (2012) Stem cell therapy in neurodegenerative diseases: from principles to practice. *Neural Regen Res* 7:1822–1831
- Scheperjans F, Aho V, Pereira PAB, Koskinen K, Paulin L, Pekkonen E, Haapaniemi E, Kaakkola S, Eerola-Rautio J, Pohja M, Kinnunen E, Murros K, Auvinen P (2015) Gut microbiota are related to Parkinson's disease and clinical phenotype. *Mov Disord* 30:350–358
- Segata N, Izard J, Waldron L, Gevers D, Miropolsky L, Garrett WS, Huttenhower C (2011) Metagenomic biomarker discovery and explanation. *Genome Biol* 12:R60
- Shan J, Qu Y, Wang S, Wei Y, Chang L, Ma L, Hashimoto K (2021) Regulation of neurotoxicity in the striatum and colon of MPTP-induced Parkinson's disease mice by gut microbiome. *Brain Res Bull* 177:103–110
- Shannon KM, Keshavarzian A, Dodiya HB, Jakate S, Kordower JH (2012) Is alpha-synuclein in the colon a biomarker for premotor Parkinson's disease? Evidence from 3 cases. *Mov Disord: Off J Mov Disord Soc* 27:716–719
- Shinno-Hashimoto H, Hashimoto Y, Wei Y, Chang L, Fujita Y, Ishima T, Matsue H, Hashimoto K (2021) Abnormal composition of microbiota in the gut and skin of imiquimod-treated mice. *Sci Rep* 11:11265
- Soares S, Soares S, Brandão E, Guerreiro C, Mateus N, de Freitas V (2020) Oral interactions between a green tea flavanol extract and red wine anthocyanin extract using a new cell-based model: insights on the effect of different oral epithelia. *Sci Rep* 10:12638
- Soliman H, Theret M, Scott W, Hill L, Underhill TM, Hinz B, Rossi FMV (2021) Multipotent stromal cells: one name, multiple identities. *Cell Stem Cell* 28:1690–1707
- Svensson E, Horváth-Puhó E, Thomsen RW, Djurhuus JC, Pedersen L, Borghammer P, Sørensen HT (2015) Vagotomy and subsequent risk of Parkinson's disease. *Ann Neurol* 78:522–529
- Teixeira MD, Souza CM, Menezes AP, Carmo MR, Fonteles AA, Gurgel JP, Lima FA, Viana GS, Andrade GM (2013) Catechin attenuates behavioral neurotoxicity induced by 6-OHDA in rats. *Pharmacol Biochem Behav* 110:1–7
- Torres ERS, Akinyeje T, Stagaman K, Duvoisin RM, Meshul CK, Sharpton TJ, Raber J (2018) Effects of sub-chronic MPTP exposure on behavioral and cognitive performance and the microbiome of wild-type and mGlu8 knockout female and male mice. *Front Behav Neurosci* 12:140
- Travagli RA, Browning KN, Camilleri M (2020) Parkinson disease and the gut: new insights into pathogenesis and clinical relevance. *Nat Rev Gastroenterol Hepatol* 17:673–685
- Venkataramana NK, Pal R, Rao SA, Naik AL, Jan M, Nair R, Sanjeev CC, Kamble RB, Murthy DP, Chaitanya K (2012) Bilateral transplantation of allogenic adult human bone marrow-derived mesenchymal stem cells into the subventricular zone of Parkinson's disease: a pilot clinical study. *Stem Cells Int* 2012:931902
- Wang S, Qu Y, Chang L, Pu Y, Zhang K, Hashimoto K (2020) Antibiotic-induced microbiome depletion is associated with resilience in mice after chronic social defeat stress. *J Affect Disord* 260:448–457
- Wang S, Ishima T, Qu Y, Shan J, Chang L, Wei Y, Zhang J, Pu Y, Fujita Y, Tan Y, Wang X, Ma L, Wan X, Hammock BD, Hashimoto K (2021) Ingestion of *Faecalibaculum rodentium* causes depression-like phenotypes in resilient *Ephx2* knock-out mice: a role of brain–gut–microbiota axis via the subdiaphragmatic vagus nerve. *J Affect Disord* 292:565–573

- Westfall S, Caracci F, Estill M, Frolinger T, Shen L, Pasinetti GM (2021) Chronic stress-induced depression and anxiety priming modulated by gut-brain-axis immunity. *Front Immunol* 12:670500
- Yemula N, Dietrich C, Dostal V, Hornberger M (2021) Parkinson's Disease and the gut: symptoms, nutrition, and microbiota. *J Parkinsons Dis* 11:1491–1505
- Zhang Y, Liu Y, Liu H, Tang WH (2019) Exosomes: biogenesis, biologic function and clinical potential. *Cell Biosci* 9:19–19
- Zhong W, Li Q, Xie G, Sun X, Tan X, Sun X, Jia W, Zhou Z (2013) Dietary fat sources differentially modulate intestinal barrier and hepatic inflammation in alcohol-induced liver injury in rats. *Am J Physiol Gastrointest Liver Physiol* 305:G919-932
- Zhou T, Yuan Z, Weng J, Pei D, Du X, He C, Lai P (2021) Challenges and advances in clinical applications of mesenchymal stromal cells. *J Hematol Oncol* 14:24

Publisher's note Springer Nature remains neutral with regard to jurisdictional claims in published maps and institutional affiliations.

Springer Nature or its licensor (e.g. a society or other partner) holds exclusive rights to this article under a publishing agreement with the author(s) or other rightsholder(s); author self-archiving of the accepted manuscript version of this article is solely governed by the terms of such publishing agreement and applicable law.